MATERIALS SCIENCE

Extreme long-lifetime self-assembled monolayer for air-stable molecular junctions

Ningyue Chen[1]†, Shuwei Li[2,3]†, Peng Zhao[1]†, Ran Liu[4]‡, Yu Xie[1], Jin-Liang Lin[1], Christian A. Nijhuis[5], Bingqian Xu[4], Liang Zhang[2,3]*, Huaping Xu[1]*, Yuan Li[1]*

The molecular electronic devices based on self-assembled monolayer (SAM) on metal surfaces demonstrate novel electronic functions for device minimization yet are unable to realize in practical applications, due to their instability against oxidation of the sulfur-metal bond. This paper describes an alternative to the thiolate anchoring group to form stable SAMs on gold by selenides anchoring group. Because of the formation of strong selenium-gold bonds, these stable SAMs allow us to incorporate them in molecular tunnel junctions to yield extremely stable junctions for over 200 days. A detailed structural characterization supported by spectroscopy and first-principles modeling shows that the oxidation process is much slower with the selenium-gold bond than the sulfur-gold bond, and the selenium-gold bond is strong enough to avoid bond breaking even when it is eventually oxidized. This proof of concept demonstrates that the extraordinarily stable SAMs derived from selenides are useful for long-lived molecular electronic devices and can possibly become important in many air-stable applications involving SAMs.

INTRODUCTION

As we approach the fundamental limit of electronic device size, a critical need to create high-performance nanodevices for efficient utilization of space and energy is unmet. Recently, novel functional devices are achieved via a complete reimagining of molecular-scale devices that are based on electron tunneling through a single molecule or a self-assembled monolayer (SAM) between two electrodes (*1*–*4*). In particular, molecular electronics implemented by SAMs are the most promising molecular device designs for practical applications (*5*, *6*). The 2022 Kavli prize has been awarded to research dedicated to developing SAMs because SAMs make it possible to control surfaces and find applications in all areas of nanoscience and nanotechnology (*7*–*11*). Nevertheless, the quality of SAMs greatly affects the performance of molecular electronics since the current density for molecular junctions is quite sensitive to the structure of SAMs (*6*, *12*). Thus, to obtain molecular electronics with excellent performance, every component of the structure is required to be optimally selected. The SAMs can be formed on either metallic electrodes or nonmetallic ones. Normally, SAMs on nonmetallic electrodes have stronger stability in the air due to the inertness of the strong covalent bond (*13*–*15*). Although stable molecular junctions can be obtained with molecules anchored with covalent chemistry, the stability, and self-assembly of SAMs contradict each other to a certain extent. SAMs with extremely strong stability structures usually have poor self-assembly and self-repair due to their strong covalent bonds. Thus, there is a trade-off between the stability and quality of SAMs (*16*). The SAMs on metallic electrodes, formed with weaker bonds and more densely packed, have some other irreplaceable advantages. For example, they can be used for surface plasmon in molecular devices (*17*) or the studies of biomolecular interaction (*18*) and also have superiority in molecular-level organic spintronic devices (*19*). There are various anchoring groups used to fabricate SAMs for metallic SAMs like amines (*20*, *21*), alkynes (*22*, *23*), ferrocenes (*24*), etc. Among those different anchoring groups, SAMs based on metal-thiolate bonds are quite well known and widely studied because they can be spontaneously organized into well-ordered single-molecular layers on various metal surfaces (of which Au, Ag, and Pt, for example, are the most widely investigated) (*10*) and form SAMs with the mostly densely packed phase, while other nontraditional ones have shortcomings to some extent like weak bonds for amines or low surface coverage for ferrocenes (*24*–*26*). This makes sulfur (S) metal chemistry the easiest method to attach molecules on top of a metal surface for the creation of complicated molecular electrical circuits, and also, the most structurally optimal one. However, the limitations of SAMs based on S-metal chemistry, are beginning to surface. One shortcoming comes from the short-term stability of thiol-based SAMs which originates from the rapidly degraded S-M (M = metal) bond under ambient conditions in the presence of oxygen, resulting in an unwanted disruption in SAMs structure or even desorption of the SAMs from metal surface (*27*, *28*). This restriction of lifetime prohibits high-performance SAM-based electronic devices outside of the laboratories, such as molecular diodes (*29*–*31*), molecular memristors (*32*–*34*), flexible transistors (*35*–*37*), etc. There are some other attempts for the antioxidation of S—M bonds by constructing well-airtight architecture in device form. The lifetime of those devices can be impressively long with more than years (*38*), while these cases cannot simulate the open

[1]Key Laboratory of Organic Optoelectronics and Molecular Engineering and Laboratory of Flexible Electronics Technology, Department of Chemistry, Tsinghua University, Beijing 100084, China. [2]Center for Combustion Energy, Tsinghua University, Beijing 100084, China. [3]School of Vehicle and Mobility, and State Key Laboratory of Intelligent Green Vehicle and Mobility, Tsinghua University, Beijing 100084, China. [4]School of Electrical and Computer Engineering, University of Georgia, Athens, GA 30602, USA. [5]Hybrid Materials for Opto-Electronics Group, Department of Molecules and Materials, MESA+ Institute for Nanotechnology, Molecules Centre and Centre for Brain-Inspired Nano Systems, Faculty of Science and Technology, University of Twente, 7500 AE Enschede, Netherlands.
*Corresponding author. Email: zhangbright@tsinghua.edu.cn (L.Z.); xuhuaping@mail.tsinghua.edu.cn (H.X.); yuanli_thu@tsinghua.edu.cn (Y.L.)
†These authors contributed equally to this work.
‡Present address: Biodesign Center for Bioelectronics and Biosensors, School of Electrical, Computer and Energy Engineering, Arizona State University, Tempe, AZ 85287, USA.

system condition in applications with oxygen around. Therefore, alternatives to S—M chemistry that can avoid degradation caused by oxidation are highly desirable. In this work, we introduce selenides as the anchoring group to be an alternative for thiols to form quality SAMs with air stability of more than 200 days, a stable alternative for SAM-based junctions (*39*–*41*).

There are efforts to search for alternative approaches. For example, SAMs of *N*-heterocyclic carbenes (NHCs) on coinage metals for molecular electronics have attracted extensive attention because of their high stability that can endure extreme pH or high-temperature (*41*, *42*). Unfortunately, the quality of monolayers is inferior due to the formation of the loosely packed phase (*41*) of NHCs SAMs owning to insufficiency of time for the self-organizing to reach the lowest surface energy based on quick carbene-metal reaction. This is why S—M chemistry seems impossible to be replaced because the ability of "self-assembly" requires the weak molecule-surface bonds that give molecules freedom to "move around" on the surface reaching the lowest free Gibbs energy for best-packing structures. Recently, Qiu *et al.* (*43*) used tunneling measurement to propose robust, air-stable SAMs of fullerene (C_{60}) functionalized triethylene glycol (PTEG-1) alternative to thiolates. Nevertheless, the devices only survived ~30 days, and an about 80% lower surface coverage (8.5×10^{13} molecule·cm^{-2}) of PTEG-1 SAMs compared to alkanethiolates SAMs (4.7×10^{14} molecule·cm^{-2}) (*44*) has been reported owing to the large volume of C_{60}. Collectively, to replace the S—M bond for better SAM-based molecular junctions, one faces a trade-off between the desire to enhance the stability by stronger bonds and the need to maintain the high quality of well-ordered SAMs.

Thiols can also be challenging to be stored since they are easily oxidized into the respective disulfides or oxysulfides in air and form impurities, leading to inferior quality relative to those derived from pure thiols (*45*, *46*). Therefore, they are often stored as their disulfide analogue or in a protected form (e.g., thioacetate derivatives) (*47*, *48*). The disulfide and thioacetate can also form SAMs, but the packing density of those SAMs is lower than thiol-formed SAMs (*49*).

For the reasons above, we hypothesize that alternative anchoring groups must have similar chemical properties of thiols (to form high-quality monolayers with low defects) while improving the stability of SAMs in ambient conditions by manipulating the interaction between the anchoring groups and the substrates. There is a suitable candidate for the alternative of thiols indeed. According to the same valence electron configurations, Se can also self-assemble on metal as S does (*50*–*53*). The difference between S and Se in the van der Waals radius, which is 1.85 Å for S and 2.0 Å for Se (*54*, *55*), enhances the binding energy of Se—Au by ≥0.25 eV stronger than the corresponding S—Au bond (*56*). The stronger bonds of Se—Au speculated from its atomic and electronic structure have been proved (*57*). Although the thermal stability of the Se-SAMs shows comparable experimental results to S-SAMs (*58*), the decisive factor of whether SAM-based molecular devices can be really put into the

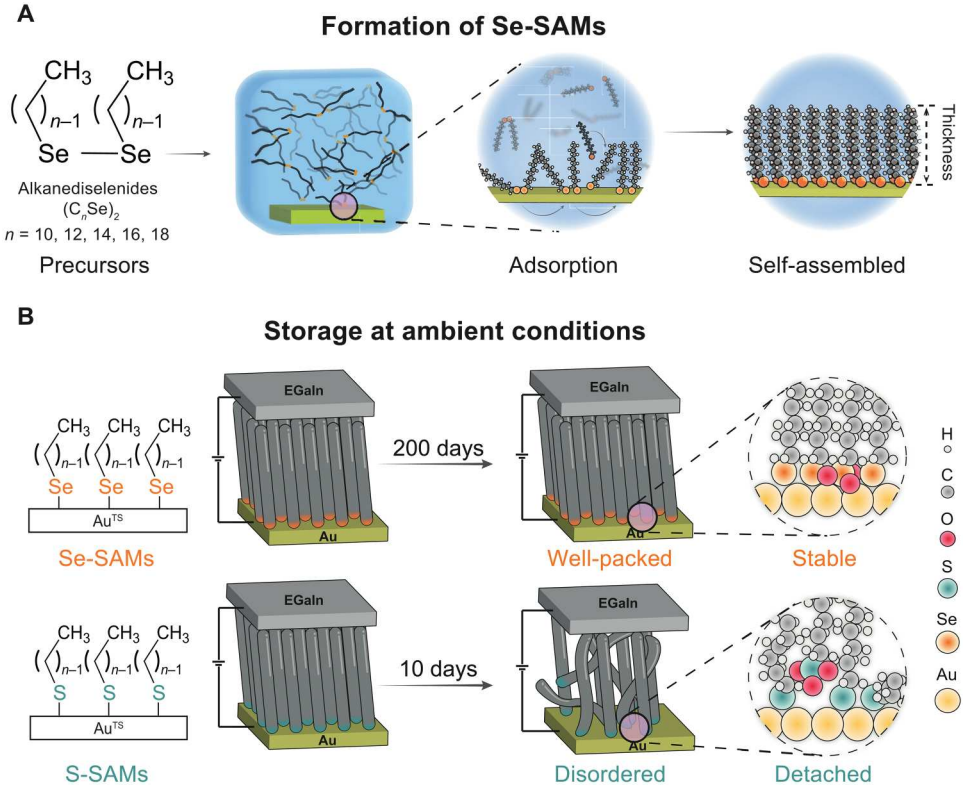

Fig. 1. Schematic of Se-SAMs formation and air-stability. (**A**) The design of precursors of Se-SAMs and schematic illustration of the process of formation of Se-SAMs. The thickness of the SAMs is defined as the length from the surface of the bottom electrode to the end of the molecule. (**B**) Schematic illustration of structure evolution of Se-SAMs and S-SAMs when stored in ambient conditions over 200 days for Se-SAMs (top) and over 10 days for S-SAMs (bottom). Au, Se, S, O, C, and H atoms are shown as yellow, orange, cyan, red, gray, and white balls, respectively.

application is the air stability. While up to now, the air stability of Se-based SAMs inside molecular junctions has not been investigated.

The goal of this work is to present SAMs anchored by Se own better air stability than SAMs anchored by S in molecular junctions. Here, we introduce long-lifetime SAMs for molecular junctions formed by the anchoring group of selenides on Au^{TS} (TS = template stripped) surfaces (abbreviated as Se-SAMs) under the same conditions as the formation of SAMs derived from thiolates (abbreviated as S-SAMs). The SAM-based molecular junctions require the highest quality of SAMs. We chose to use diselenides as the precursors instead of using selenols directly because of their stronger oxidation resistance ability and based on the studies that the Se—Se bonds near Au surfaces, as dynamic covalent bonds, can break and form Se—Au bonds to pack as high-quality SAMs on the substrates (*54*, *59*–*61*). The high-quality Se-SAMs were grown by immersion of gold surfaces in a solution of diselenides as shown in Fig. 1A (see Materials and Methods), and these SAMs exhibited long stability compared to S-SAMs due to their weaker binding affinity to oxygen and would not desorb (Fig. 1B). The S-SAMs, on the other hand, suffered from oxidation of S into disulfides and sulfonates, leading to the loss of electrical properties for only 10 days (fig. S1). To fully compare with the extensively studied S-SAMs, we synthesized five different chain lengths of *n*-alkanediselenides of the form of $[CH_3(CH_2)_{n-1}Se]_2$ (*n* stands for the number of carbon atoms) with *n* = 10, 12, 14, 16, and 18 [abbreviate as $(C_nSe)_2$, Fig. 1A] to grow Se-SAMs on gold. The quality of the SAMs was characterized by scanning tunneling microscopy (STM) and x-ray photoelectron spectroscopy (XPS). We measured the tunneling current passing through SAMs to monitor the possible subtle changes in the quality of the SAMs over 200 days under ambient conditions because tunneling barriers defined by the SAMs are highly sensitive to defects. The tunneling currents did not change over 200 days, from which we conclude that the SAMs anchored

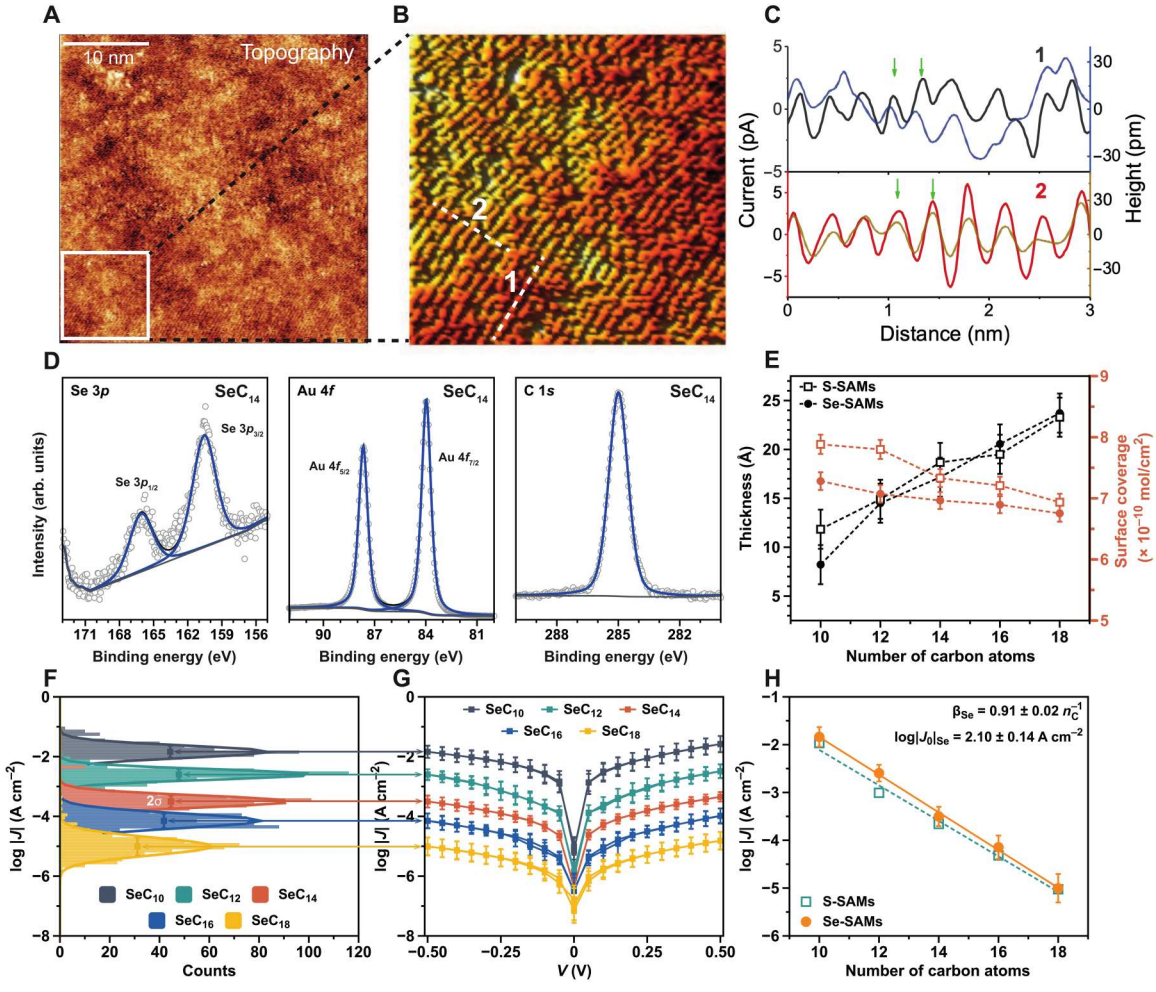

Fig. 2. Characterization of Au-SeC$_n$ by STM, XPS, and tunneling current measurements. (**A**) STM topography of Au-SeC$_{14}$ SAMs on mica. (**B**) Image of the region marked by the rectangle in (A). The white dashed lines 1 and 2 correspond to molecular alignment directions 1 and 2, respectively. (**C**) The current and height profiles for 1 and 2 [corresponding to the white dashed lines in (B)]. (**D**) XPS data (Se 3*p*, Au 4*f*, and C 1*s*) of freshly prepared Au-SeC$_{14}$. (**E**) The thickness and surface coverage of Se-SAMs and S-SAMs as the function of carbon numbers derived from XPS. (**F**) The histograms of log |*J*| at −0.50 V with Gaussian fits for Au-SeC$_n$//Ga_2O_3/EGaIn junctions. (**G**) Plots of the log |*J*| curves for Au-SeC$_n$//Ga_2O_3/EGaIn junctions. The peak of the Gaussian in (F) gives the log-mean value of *J* (log |*J*|), shown at *V* = −0.5 V as one point on the average trace (G), while the log-SD (σ_{log}) of the Gaussian in (F) provides the error bars for the same point. (**H**) Plots of log |*J*| at −0.50 V versus n_C for Au-SeC$_n$//Ga_2O_3/EGaIn junctions and Au-SC$_n$//Ga_2O_3/EGaIn junctions. *n* = 10, 12, 14, 16, and 18.

by Se own better air stability than SAMs anchored by S. Our theoretical calculations suggest that the superior stability of Se-SAMs originates from the stronger Se—Au interaction and weak oxygen affinity. Our results also indicate oxidation of the Se—Au bond does not lead to notable disruption of the Se-SAM structure, explaining the extraordinary stability of the Se-SAMs. Our results demonstrate that the Se-SAMs are promising alternatives to conventional S-SAMs for applications in SAM-based molecular junctions because the Se anchoring group is much more stable yet the overall SAMs structure and associated chemistry are very similar to that of S (unlike other approaches where the anchoring group substantially affects chemistry and structure of the SAMs). This improved stability makes Se-SAMs interesting not only for molecular electronics but also for a wide range of applications in nanotechnology.

RESULTS

Se-SAMs characterization

The reaction energy profile (fig. S2) calculated by density functional theory (DFT) shows that $(SeCH_3)_2$ has stronger binding energy and substantially lower Se—Se dissociation energy barrier than $(SCH_3)_2$ on Au (111) surface, suggesting that diselenides are appropriate precursors for stable SAMs by avoiding the disordered phases caused by physisorption (*62*). On the basis of the theoretical prediction, we experimentally conducted STM imaging of SeC_{14}-SAMs formed on Au and a highly ordered phase can be seen in Fig. 2 (A and B). The height profile peaks (Fig. 2C) indicate the successful formation of SeC_{14}-SAMs with a coverage density of ~10 molecules · nm^{-2} that is in good agreement with S-SAMs (see fig. S3). Next, we used XPS to further analyze the chemical environment of elements and the nature of the bonds of Se-SAMs more accurately. Because the binding energy of Se 3*d* peak overlaps with the Au 5*p* peak (see fig. S4), we measured Se 3*p* spectra to analyze the chemical environment and relative content of Se in the SAMs. All high-resolution Se 3*p*, Au 4*f*, C 1*s*, and O 1*s* spectra of all Se-SAMs can be found in fig. S5. We took SeC_{14}-SAMs as an example to illustrate the peak assignment in Fig. 2D (the spectra of Se 3*p*, Au 4*f*, and C 1*s* respectively). The Se 3*p* spectrum exhibits a single Se $3p_{1/2,3/2}$ doublet, which indicates the Se—Se bonds only form Se—Au bonds from the cleavage of Se—Se. This observation is in good agreement with other groups using Se—Se to form Se-SAMs (*57*, *63*), and therefore, we attributed the binding energy of 160.4 eV of Se $3p_{3/2}$ to chemisorbed Se to the Au surface. The 84.0 eV of Au 4*f* and 284.8 eV of C 1*s* can be assigned to Au-atoms in bottom electrodes and C-atoms in alkyl chains. We then calculated the thickness and surface coverage from the results of XPS and all the results showed that the Se-SAMs yield high-quality SAMs with similar packing density and thickness (Fig. 2E) with a detailed description of the calculation of thickness and surface coverage provided in Materials and Methods (table S1). In addition, the water contact angles of SeC_n-SAMs and SC_n-SAMs are very similar, implying that the surface free energy of those two kinds of SAMs are kindred (fig. S6 and table S2).

Using tunneling to examine the quality of the Se-SAMs

Here, we used a eutectic liquid metal of a gallium and indium alloy (so-called EGaIn; covered with a native 0.7-nm-thick layer of Ga_2O_3) as the top electrodes to fabricate molecular junctions in the form of Au-SeC_n//Ga_2O_3/EGaIn (n = 10, 12, 14, 16, and 18) to investigate the electrical properties of Se-SAMs and compared the results with S-SAMs of equivalent length. The tunneling current (I) passing through SAMs exponentially decays over distance d (represented by n_C) with a decay coefficient (β) that is proportional to the square root of the tunneling barriers. When the medium of tunneling consists of alkyl chains, this relationship fits the general simplified model (for linear potential drops)

$$I/A = J = J_0 e^{-\beta d} \quad (1)$$

where A (cm^2) is the contact area between the electrodes and SAMs, J ($A \cdot cm^{-2}$) is the current density, d is the thickness of the SAMs, and J_0 is a constant that depends on the contacts and system. We recorded statistically large numbers (>500) of J(V) curves to plot the histograms of log J at all applied voltages V to obtain log-mean values of J (log |J|) and its corresponding log-standard deviation (σ_{log}) (Fig. 2F). Besides, Fig. 2G shows log |J|(V) curves for junctions of Au-SeC_n//Ga_2O_3/EGaIn constructed by the log |J| and σ_{log} versus V. We found a narrow distribution of log |J| for all samples ($\sigma_{log} < 0.6$), demonstrating the uniformity and stability of Se-SAMs. To thoroughly compare the impact of replacing anchoring groups, we analyzed the log |J| as a function of n_C and fitted the data to eq 1 (Fig. 2H). The values of β = 0.91 ± 0.02 n_C^{-1} and log |J_0| = 2.10 ± 0.14 obtained for Se-SAMs are close to those of S-SAMs (β = 0.87 ± 0.03 n_C^{-1} and log |J_0| = 1.78 ± 0.18) and other SAMs composed of the alkyl chain formed by the nonthiolates system, NHCs (*64*), carboxyl (*65*), and alkyne (*66*). Thus, these junctions behave within error essentially the same and therefore we conclude that Se-SAMs form very similar tunneling barriers as Se-SAMs in agreement with the characterization results described above, from which we concluded that both types of SAMs have similar packing densities and heights. Yet, for precursors of disulfides, the current density with huge distributions is quite larger than SAMs formed by thiols and diselenides (fig. S7) and the yields of them are also much lower (table S3).

The lifetime of Se-SAM junctions

To test the lifetime of the junctions with Se-SAMs, we prepared over 40 samples for each length of the molecules (200 in total for n = 10, 12, 14, 16, and 18) and stored all samples inside a dry box with air and in the dark, which helps to minimize the impurities adsorption from the environment. Every 10 days, we randomly took samples to conduct the junction test by recording data from 10 junctions (240 traces) for each type of SAMs to calculate log |J| and plot the log |J| (V) curves as described earlier (see Materials and Methods for details and statistical analysis). For the control experiment of the stability of S-SAMs, we chose SC_{10}-SAMs as an example and did junction test after storing them in the same environment as Se-SAMs, and the results of rapidly increasing current density are given in fig. S1. All histograms of log |J| at −0.50 V with Gaussian fits for all Au-SeC_{14}//Ga_2O_3/EGaIn junctions over 200 days are shown in Fig. 3A, which indicates the steadiness of value of J and also the large amount of data (see fig. S8 for histograms of log |J| at −0.50 V with Gaussian fits for the other four Se-SAMs). The vertical black dashed lines in Fig. 3A indicate the log |J| corresponding to the orange square in Fig. 3B, and the horizontal black double arrows indicate σ_{log} corresponding to the orange error bar in Fig. 3B. The results in Fig. 3B show that the average current density of five kinds of Se-SAMs did not change during this period (see fig. S9 for all

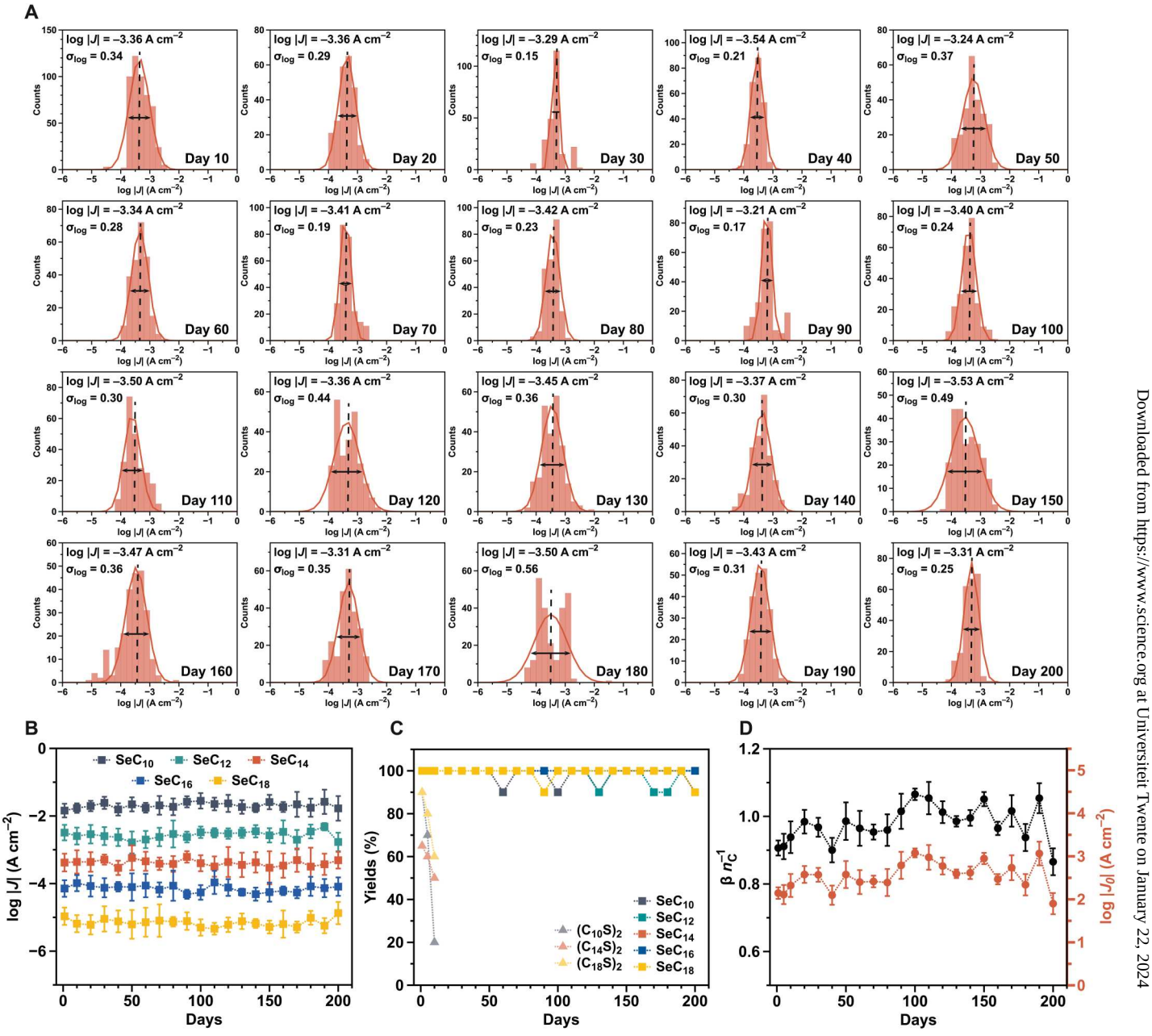

Fig. 3. The lifetime of Au-SeC$_n$ monitored by tunneling. (**A**) An example of the histograms of log |*J*| at −0.50 V with Gaussian fits for all Au-SeC$_{14}$//Ga$_2$O$_3$/EGaIn junctions measured every 10 days. (**B**) Plots of the log |*J*| at −0.50 V for Au-SeC$_n$//Ga$_2$O$_3$/EGaIn junctions as a function of days. (**C**) Yields of Au-SeC$_n$//Ga$_2$O$_3$/EGaIn junctions as a function of days. n = 10, 12, 14, 16, and 18; yields of Au-(C$_n$S)$_2$//Ga$_2$O$_3$/EGaIn junctions as a function of days. n = 10, 14, and 18. (**D**) Values of β and log |J_0| measured as a function of days. All samples were kept under ambient conditions.

traces). All junctions [1100 junctions and 52,800 individual *J*(V) traces in total] were stable and obtained with high yields (Fig. 3C). The values of β and log |J_0| shown in Fig. 3D also fluctuated within the range commonly reported by others, which indicates a stationary tunneling barrier of every sample over 200 days (additional values of β fits are described in fig. S10). Therefore, we conclude from the tunneling data that the overall packing and heights of the Se-SAMs stayed unchanged in 200 days. To exclude the possibility that stability arises from the diselenides precursors, we conducted a comparative experiment using other dichalcogenides, alkyl chains with disulfide head groups. It can be observed that the yield of junctions formed by C$_n$-disulfide SAMs sharply decreased within 10 days (Fig. 3C; see current densities results in fig. S11) under ambient conditions and 3 days in pure O$_2$ (fig. S11), indicating their inability to maintain the stability of their electrical properties. The electrochemical results further confirm that as the oxidation process deepens, the S—Au bonds strength in the disulfide SAMs gradually weakens, accompanied by the formation of more

pinholes. In contrast, the bond strength and regularity in the Se-SAMs remain unchanged (figs. S12 and S13). Therefore, the stability of Se-SAMs is attributed to the interaction between the anchoring groups and the gold substrate.

Oxidation of Se-SAMs under ambient conditions

The most interesting phenomenon we found is that the Se-SAMs are more stable against oxidations than S-SAMs, yet they still can be oxidized slowly under ambient conditions. The whole oxidation process was monitored by XPS as a function of time for 200 days. Our XPS analysis showed that the oxidation of the Se—Au bond, unlike the S—Au bond of the S-SAMs, did not lead to the breaking and associated desorption of the Se—Au bond. The O 1*s* peak around 532 eV appeared in every sample, but this was commonly observed with samples prepared under ambient conditions and, therefore, we assigned this signal to contamination by adventitious material physically adsorbed on the surface (*67*). For Se 3*p* spectra, a new doublet emerged at 162.5 eV (yellow line labeled as Se_{oxi} in Fig. 4A for SeC_{10} and Fig. 4C for SeC_{14}), which was close to the binding energy of Se IV (*68*). Along with the new doublet in Se 3*p* spectra, a new peak emerged in the O 1*s* spectrum at 531.7 eV (labeled as O_{Se} in Fig. 4B for SeC_{10} and Fig. 4D for SeC_{14}). The appearance and change of content of peak at 531.7 eV are correlated to the new doublet of Se 3*p*, revealing that the increase of valence state of Se was caused by forming Se—O bond on the surface. To quantitatively characterize these data, we integrated the peak area to obtain the elemental ratio of Se/Au and O/Au of the SeC_{10} (Fig. 4E) and SeC_{14} SAMs (Fig. 4F). The oxidations of the Se—Au bond started from 60 to 80 days for SeC_{10}-SAMs and around 150 days for SeC_{14}-SAMs and by the comparison of data of all five SAMs, we found for SAMs with different *n* that this oxidation process was faster for small values of n than for large values (the new peaks appeared around 200 days for SeC_{18}-SAMs; see fig. S14 for XPS data for the other three kinds of SAMs). Yet, the overall amounts of Se remained nearly unchanged within experimental uncertainties for both small and large values of n (see fig. S15 for

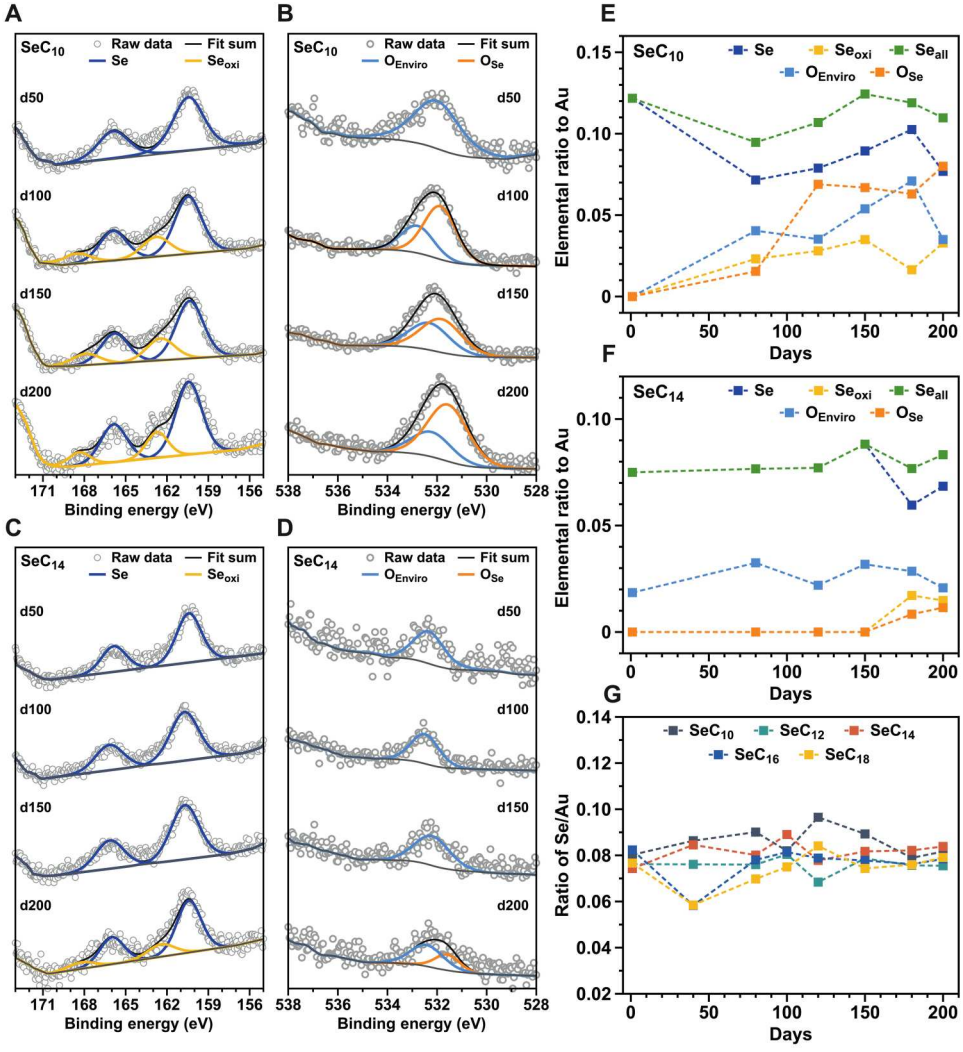

Fig. 4. The oxidation process of Au-SeC_n monitored by XPS. (**A**) Se 3*p* peak spectrum for Au-SeC_{10}. (**B**) O 1*s* peak spectrum for Au-SeC_{10}. (**C**) Se 3*p* peak spectrum for Au-SeC_{14}. (**D**) O 1*s* peak spectrum for Au-SeC_{14}. The relative ratio of O and Se to Au from XPS Au-SeC_{10} (**E**) and Au-SeC_{14} (**F**) as a function of days. (**G**) Se/Au ratio of Au-SeC_n (*n* = 10, 12, 14, 16, and 18) derived from XPS results as a function of days.

monitoring of elemental ratio for the other three kinds of SAMs). These observations indicated that the Se—Au bonds were strong enough to prevent, unlike S-SAMs, desorption from the Au surface even after oxidation. Another key feature of the air ability of Se-SAMs was the ratio of Se/Au of Au-SeC_n (n = 10, 12, 14, 16, and 18) changed within 10% errors (Fig. 4G). This was a clear indication that the value of the surface coverage of Se-SAMs remained unchanged. That is, there was almost neither desorption nor substantial structural changes over 200 days of ageing of the Se-SAMs. Our data point toward a potential role of Se-SAMs with strong durability under ambient conditions without being damaged by possible oxidation.

Theoretical calculations

To gain more insights into the origin behind the good stability of Se-SAMs, we performed DFT calculations (see details in Materials and Methods) to estimate the binding strength of SeC_{10} and SC_{10} on Au (111) and Au (100) surfaces (Fig. 5, A and B, table S4, and see all optimized structures of the SAMs in figs. S16 to S19). Figure 5A shows that SeC_{10} exhibits a stronger binding energy (Se, −2.18 eV; S, −2.01 eV) with the Au (111) surface and a weaker O affinity (Se, −0.56 eV; S, −0.98 eV) with respect to SC_{10} (a versus b). This binding trend confirms the enhanced Au—Se interaction observed experimentally and is also in line with the superior resistance to oxidation of Se-SAMs. The surface stability of S-SAMs and Se-SAMs are both susceptible to oxidation. However, the decrease of Se—Au binding strength (0.14 eV) is notably smaller than S—Au after oxidation (0.22 eV). Moreover, once oxidation is initiated, the oxidized S-SAMs have stronger adsorption energy with consecutive oxygen atoms (−2.14 eV), i.e., greater driving force to get further oxidized than Se—SAMs (−1.09 eV) (figs. S16 to S19). Au (100) holds a similar trend as Au (111), except for the fact that the binding strength of S—Au and Se—Au are comparable. The above DFT results reveal that the superior stability of Se-SAMs over S-SAMs (Fig. 3) can be attributed to the stronger Se—Au interaction and elevated antioxidant capacity. To further investigate the electronic-

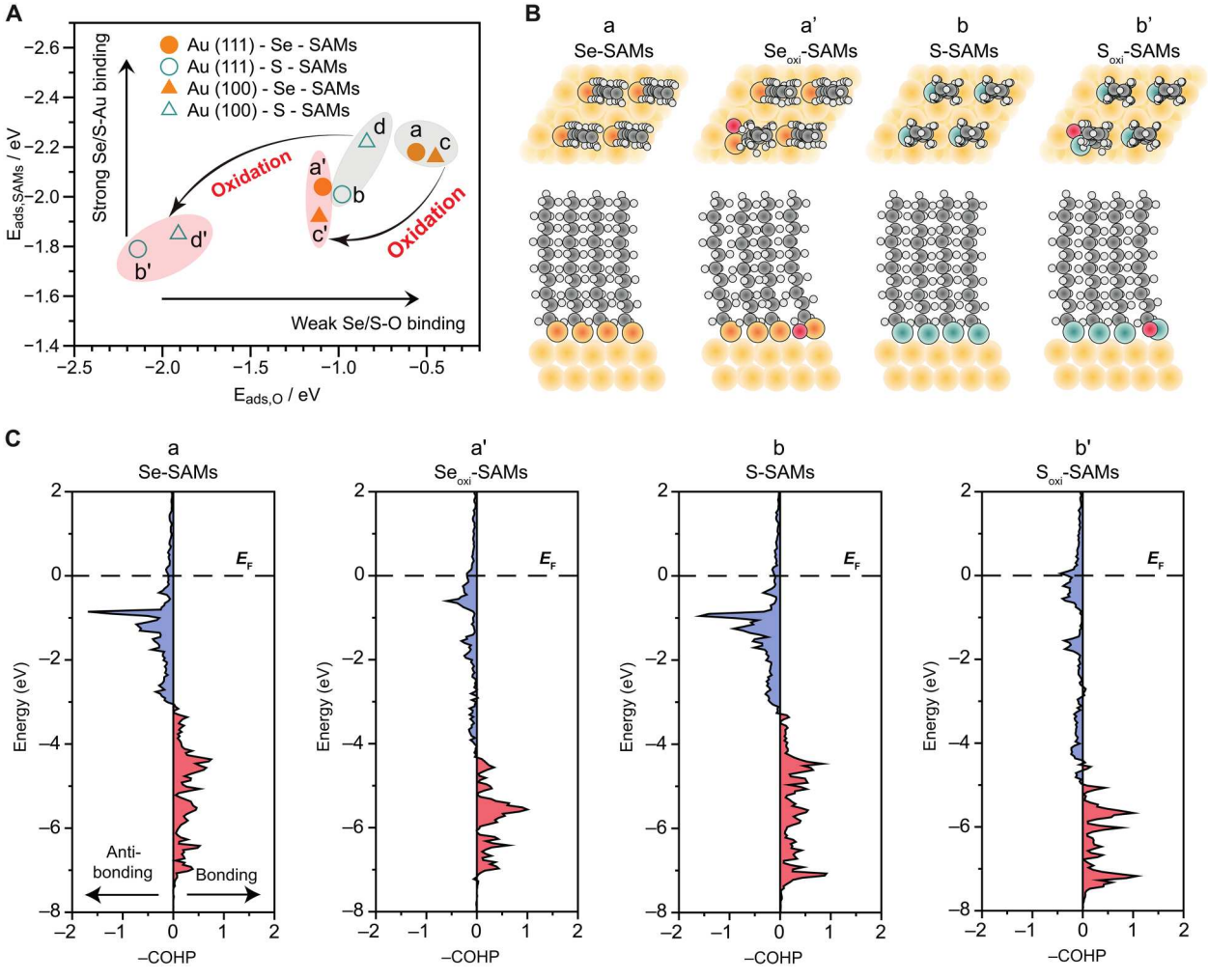

Fig. 5. DFT-calculated SeC_{10} and SC_{10} adsorption energies and the corresponding COHP. (**A**) Surface adsorption energy of SeC_{10} (or SC_{10}) plotted against Se/S—O binding energy on Au (100) (triangles) and Au (111) (circles) surfaces: SeC_{10} (a) and SC_{10} (b) on Au (111) surface, SeC_{10} (c) and SC_{10} (d) on Au (100) surface, oxidized SeC_{10} (a′) and SC_{10} (b′) on Au (111) surface, and oxidized SeC_{10} (c′) and SC_{10} (d′) on Au (100) surface. (**B**) The top view and side view of the adsorption geometries on Au (111) surface. Au, Se, S, O, C, and H atoms are shown as yellow, orange, cyan, red, gray, and white balls, respectively. (**C**) The projected crystal orbital Hamilton population (COHP) between Au *d* orbitals and Se or S *p* orbitals.

structural origin, we conducted the Au—Se/S bonding analysis by calculating crystal orbital Hamiltonian population (COHP), as shown in Fig. 5C. The COHP was used to reveal the nature of adsorption between Au *d* orbitals and Se or S *p* orbitals (*69*–*71*). The calculated COHPs were displayed by drawing negative (i.e., bonding) contributions to the right and positive (i.e., antibonding) contributions to the left. Figure 5C shows that the filling of Au—Se/S bonding orbital populations decreases when an oxygen atom adsorbed on Se or S (A→A′, B→B′), which is in accordance with the decrease of binding strength for SeC_{10} and SC_{10} after oxidation on Au (111) surface as depicted in Fig. 5A. However, the decrease of Au-SeC_{10} is smaller than that of the Au-SC_{10}, as indicated by the difference of the integrated COHP value (Se, −0.05 eV; S, −0.07 eV), demonstrating the higher antioxidant capacity and thus a potential longer lifetime.

DISCUSSION

We have successfully fabricated high-quality SAMs from the precursors of *n*-alkanediselenides, and shown that the Se—Au bond is strong enough to resist desorption by oxidation in air rather than the readily oxidized and broken S—Au bond. This property resulted in long-lived Se-SAM–based junctions with lifetime of 200 days. The theory supports our experimental observations and shows that the superior stability of Se-SAMs originates from the reduction of the oxidation of Se—Au bonds and the weaker effect of oxygen on the binding strength with the Au surface of SeC_{10} than that of SC_{10}. These results indicate that the anchoring groups of selenides are better than thiols with at least two profound implications. First, the thiolates compounds need to be stored in refrigerator to slow down the oxidation of —SH, but diselenides compounds as the precursors can be stored in the air, which is a huge benefit for easy handling and reproducibility of experiments. Second, the strong Se—Au bond can resist desorption upon oxidations and our DFT calculations suggest that the Se—Au bond will not break after oxidation by three oxygen atoms (figs. S20 to S21), theoretically indicating a possible much longer lifetime of Se-SAMs than we experimentally monitored so far (fig. S22; we found that they are still electrically stable >300 days). The advantage of using Se as the anchoring group over other approaches (usually requiring bulkier groups) is that the supramolecular structure of the SAMs is not disturbed and that the same methods as developed for the very well-known thiol anchoring groups can be used to form the SAMs. For these reasons, we believe that our approach will be an important step further toward applications of molecular electronics and benefit all areas of research involving SAMs on metal surfaces.

MATERIALS AND METHODS

Template-stripped bottom electrodes (Au^{TS})

We fabricated the template-stripped bottom electrodes following the previous reports (*72*). We used gold pellets [0.125″ (diameter) × 0.125″ (length)] with the purity of 99.999% obtained from Dimu Materials Inc. (China). Silicon (100, p-type) wafers are from KST (Japan), with a thickness of 525 ± 25 μm with one side polished. We used a thermal deposition (Shen Yang Ke Yi, China) to deposit Au vapor on top of polished surfaces of Si/SiO_2 wafers. The vacuum of deposition was about 8×10^{-5} Pa, and the evaporation rate was about 0.2 Å/s at the first 50 nm and then increased to ~1 Å/s for the rest 150 nm. The glass slides (1.5 × 1.5 cm^2) were ultrasonically cleaned with acetone and then ethanol for 20 min, and the slides were blown to dryness in a stream of N_2 gas. After we cleaned the glass slides with a plasma of air for 5 min at a pressure of 100 Pa, the glass slides were glued on the Au surfaces by photo-curable optical adhesive (Norland, no. 61). A 100-W ultraviolet lamp was used to cure the optical adhesive for 1 hour at a distance of 60 cm from the light source. The Au surface that had been in contact with the Si/SiO_2 wafer was lift-off by a razor blade.

Formation of Se-SAMs

We synthesized didecyl diselenide $(C_{10}Se)_2$, didodecyl diselenide $(C_{12}Se)_2$, ditetradecy diselenide $(C_{14}Se)_2$, dihexadecyl diselenide $(C_{16}Se)_2$, and octadecyl diselenide $(C_{18}Se)_2$ through the reaction of disodium diselenide and bromoalkenes of corresponding length (*73*) (see synthesis details in figs. S23 to S27). The Se-SAMs were formed by immersion of freshly prepared substrates into a 5 μM $[CH_3(CH_2)_{n-1}Se]_2$ with n = 10, 12, 14, 16, and 18 solutions in absolute ethanol at room temperature. After immersion of 24 hours, the samples were carefully rinsed with pure ethanol and then blown dry with argon gas. For the control samples of S-SAMs, we used commercial *n*-alkanethiolates from Adamas and fabricated S-SAMs under similar conditions with concentrations and time of formation, which is also widely used by others (*9*).

STM imaging

The STM images were obtained by scanning the $CH_3(CH_2)_{13}Se$ SAMs on a mica-Au (110) substrate with a scanning tip made of tungsten. The scanning was performed under dry conditions and at room temperature (*74*). The newly prepared gold substrates were immersed in 5 μM $[CH_3(CH_2)_{13}Se]_2$ solution for 10 hours at room temperature, using absolute ethanol as the solvent, to form Se-SAMs. The surface coverage derived from STM was calculated from the height profile of Fig. 2C, which was corresponding to the lines #1 and #2 in Fig. 2B. Since the peak height represents the existence of molecule, we can speculate there are 9 to 10 molecules per 3.0 nm, that is, 81 to 100 molecules/9.0 nm^2 (lines #1 and line #2 can represent two sides of a square on the surface) and the surface coverage of SeC_{14}-SAMs can be estimated as ~10 molecules/nm^2.

Spectroscopy measurements

XPS was conducted with the NCESBJ (National Centre of Electron Spectroscopy in Beijing). All measurements were performed in an ultrahigh vacuum chamber with a base pressure of 1×10^{-8} Pa. The energy of the incident x-ray beam (1486.6 eV) was used by the Thermo Fisher Scientific K-Alpha XPS system. We recorded survey spectra and high-resolution spectra of C 1*s*, Se 3*p*, O 1*s*, and Au 4*f*. The thickness of the monolayers can be calculated by

$$\frac{I_{C(1s)}}{I_{Au(4f)}} = k\frac{1 - e^{-d_C/\lambda_C}}{e^{-d_{CSe}/\lambda_{Au}}}$$

where I is the integrated peak area, λ_C is the escape depth of C 1*s* photoelectrons through the carbon layer, λ_{Au} is the escape depth of the Au 4*f* photoelectrons through thiolate of selenol layer, d_C is the thickness of the carbon layer, and d_{CSe} is the thickness of the selenol/thiolate layer, and k is an instrument-specific constant. For the calibration of the instrument, we calculated C_{1s}/Au_{4f} intensity ratios of all samples and compared the values with SC_{12} -SAMs

that the thickness was known (*54*) so as to obtain the thickness of all samples.

Since we have known *d*, all samples' surface coverages can be calculated. We can obtain the relative Γ_{SAM} values by comparing I_{Au} for the SAMs of different anchoring groups given by (*75*).

$$I_{0,Au} = \frac{I_{Au}}{e^{-d/\lambda}}$$

Here, $I_{0,Au}$ is the initial signal generated from the 4*f* orbital of Au atoms without attenuation over the thickness of SAMs. the value of Γ_{SAM} of SC_{10} on Au (111) surface has been reported before and is 7.8×10^{-10} mol/cm^2 (*44*). Thus, we compared the values of $I_{0,Au}$ of all SAMs against the value of $I_{0,Au}$ SC_{10} form on Au to estimate the relative Γ_{SAM} values of the SAMs in this study.

Junction measured by EGaIn technique

We used cone-shaped tips of Ga_2O_3/EGaIn as top electrodes using a previously described home-built system (*72*). This technique makes it possible to form junctions in which the electrical characteristics are dominated by the chemical and supramolecular structure of the SAMs inside the junctions and to record data with statistically large numbers. Device properties are not dominated by any of the other asymmetries, nor by the Ga_2O_3 layer, present in these junctions.

Statistical analysis

For the freshly prepared SAMs, the junctions of each type of SAM were fabricated on three different Au samples using the "EGaIn-technique." We formed seven junctions on each substrate. For each junction, we recorded 24 scans (0 V → +0.5 V → 0 V → −0.5 V → 0 V) with a step size of 50 mV and a delay of 0.1 s. We collected more than 500 traces for each type of SAMs (see table S5), and we calculated log |*J*| using previously reported methods (*72*). For the electrical stability test, we randomly chose a sample for each type of SAMs every 10 days and formed 10 junctions on these SAMs and collected 240 traces for each type of SAMs. Other analysis methods are the same as above.

Theoretical calculations

All calculations were performed via the Vienna Ab Initio simulation package using DFT (*76*, *77*). Core electrons were described using the projected-augmented wave method (*78*). The Kohn-Sham wave functions were expanded on a plane-wave basis with a kinetic energy cutoff of 400 eV to describe the valence electrons. The generalized gradient approximation using the Perdew-Burke-Ernzerhof functional was used to evaluate the exchange correlation energy (*79*). The Au (100) and Au (111) surfaces were modeled with a four-layer (2 × 4) and ($2\sqrt{3} \times 2\sqrt{3}$) unit cell, respectively, the bottom two layers of the surface were kept frozen, while the other layers and adsorbates were set free to relax. A vacuum space of >25 Å was added to all surface models to ensure no appreciable interaction between periodic images. The Monkhorst-Pack scheme was used to sample the Brillouin zone using a 5 × 3 × 1 *k*-point grid for Au(100) surface and a 3 × 3 × 1 *k*-point grid for Au(111) surface (*80*), respectively. Geometry was considered optimized when the force on each atom was <0.025 eV/Å. The COHP was obtained by LOBSTER code (*81*). The location and energy of transition states were calculated with the climbing-image nudged elastic band method (*82*, *83*).

Supplementary Materials

This PDF file includes:

Supplementary Text
Figs. S1 to S27
Tables S1 to S5
References

REFERENCES AND NOTES

1. L. J. Cui, S. Hur, Z. A. Akbar, J. C. Klockner, W. Jeong, F. Pauly, S. Y. Jang, P. Reddy, E. Meyhofer, Thermal conductance of single-molecule junctions. *Nature* **572**, 628–633 (2019).
2. J. Bai, A. Daaoub, S. Sangtarash, X. H. Li, Y. X. Tang, Q. Zou, H. Sadeghi, S. Liu, X. J. Huang, Z. B. Tan, J. Y. Liu, Y. Yang, J. Shi, G. Meszaros, W. B. Chen, C. Lambert, W. J. Hong, Anti-resonance features of destructive quantum interference in single-molecule thiophene junctions achieved by electrochemical gating. *Nat. Mater.* **18**, 364–369 (2019).
3. L. Yuan, L. J. Wang, A. R. Garrigues, L. Jiang, H. V. Annadata, M. A. Antonana, E. Barco, C. A. Nijhuis, Transition from direct to inverted charge transport Marcus regions in molecular junctions via molecular orbital gating. *Nat. Nanotechnol.* **13**, 322–329 (2018).
4. M. Y. Zhao, Y. H. Chen, K. X. Wang, Z. X. Zhang, J. K. Streit, J. A. Fagan, J. S. Tang, M. Zheng, C. Y. Yang, Z. Zhu, W. Sun, DNA-directed nanofabrication of high-performance carbon nanotube field-effect transistors. *Science* **368**, 878–881 (2020).
5. Y. Liu, X. Qiu, S. Soni, R. C. Chiechi, Charge transport through molecular ensembles: Recent progress in molecular electronics. *Chem. Phys. Rev.* **2**, 021303 (2021).
6. A. Vilan, D. Aswal, D. Cahen, Large-area, ensemble molecular electronics: Motivation and challenges. *Chem. Rev.* **117**, 4248–4286 (2017).
7. L. H. N. Dubois, R. G. Nuzzo, Synthesis, structure, and properties of model organic surfaces. *Annu. Rev. Phys. Chem.* **43**, 437–463 (1992).
8. R. G. Nuzzo, L. H. Dubois, D. L. Allara, Fundamental studies of microscopic wetting on organic surfaces. 1. Formation and structural characterization of a self-consistent series of polyfunctional organic monolayers. *J. Am. Chem. Soc.* **112**, 558–569 (1990).
9. J. C. Love, L. A. Estroff, J. K. Kriebel, R. G. Nuzzo, G. M. Whitesides, Self-assembled monolayers of thiolates on metals as a form of nanotechnology. *Chem. Rev.* **105**, 1103–1170 (2005).
10. R. G. Nuzzo, D. L. Allara, Adsorption of bifunctional organic disulfides on gold surfaces. *J. Am. Chem. Soc.* **105**, 4481–4483 (1983).
11. P. E. Laibinis, G. M. Whitesides, D. L. Allara, Y. T. T. R. G. Nuzzo, Comparison of the structures and wetting properties of self-assembled monolayers of n-alkanethiols on the coinage metal surfaces, copper, silver, and gold. *J. Am. Chem. Soc.* **113**, 7152–7167 (1991).
12. D. Thompson, C. A. Nijhuis, Even the odd numbers help: Failure modes of SAM-based tunnel junctions probed via odd-even effects revealed in synchrotrons and supercomputers. *Acc. Chem. Res.* **49**, 2061–2069 (2016).
13. A. Morteza Najarian, B. Szeto, U. M. Tefashe, R. L. McCreery, Robust all-carbon molecular junctions on flexible or semi-transparent substrates using "process-friendly" fabrication. *ACS Nano* **10**, 8918–8928 (2016).
14. A. J. Bergren, L. Zeer-Wanklyn, M. Semple, N. Pekas, B. Szeto, R. L. McCreery, Musical molecules: The molecular junction as an active component in audio distortion circuits. *J. Phys. Condens. Matter* **28**, 094011 (2016).
15. S. Seo, M. Min, S. M. Lee, H. Lee, Photo-switchable molecular monolayer anchored between highly transparent and flexible graphene electrodes. *Nat. Commun.* **4**, 1920 (2013).
16. R. L. McCreery, A. J. Bergren, Progress with molecular electronic junctions: Meeting experimental challenges in design and fabrication. *Adv. Mater.* **21**, 4303–4322 (2009).
17. W. Du, T. Wang, H. S. Chu, C. A. Nijhuis, Highly efficient on-chip direct electronic-plasmonic transducers. *Nat. Photonics* **11**, 623–627 (2017).
18. T. H. Lee, D. J. Hirst, K. Kulkarni, M. P. Del Borgo, M. I. Aguilar, Exploring molecular-biomembrane interactions with surface plasmon resonance and dual polarization interferometry technology: Expanding the spotlight onto biomembrane structure. *Chem. Rev.* **118**, 5392–5487 (2018).
19. J. Y. Hong, S. H. Chang, K. H. O. Yang, P. C. Yeh, H. W. Shiu, C. H. Chen, W. C. Chiang, M. T. Lin, A multifunctional molecular spintronic platform with magnetoresistive and memristive responses via a self-assembled monolayer. *J. Appl. Phys.* **125**, 142905 (2019).
20. S. O'Mahony, C. O'Dwyer, C. A. Nijhuis, J. C. Greer, A. J. Quinn, D. Thompson, Nanoscale dynamics and protein adhesivity of alkylamine self-assembled monolayers on graphene. *Langmuir* **29**, 7271–7282 (2013).
21. L. X. Tian, E. Martine, X. Yu, W. P. Hu, Amine-anchored aromatic self-assembled monolayer junction: Structure and electric transport properties. *Langmuir* **37**, 12223–12233 (2021).
22. S. Zhang, K. L. Chandra, C. B. Gorman, Self-assembled monolayers of terminal alkynes on gold. *J. Am. Chem. Soc.* **129**, 4876–4877 (2007).

23. D. Fracasso, S. Kumar, P. Rudolf, R. C. Chiechi, Self-assembled monolayers of terminal acetylenes as replacements for thiols in bottom-up tunneling junctions. *RSC Adv.* **4**, 56026–56030 (2014).
24. P. Song, S. Guerin, S. J. R. Tan, H. V. Annadata, X. J. Yu, M. Scully, Y. M. Han, M. Roemer, K. P. Loh, D. Thompson, C. A. Nijhuis, Stable molecular diodes based on π–π interactions of the molecular frontier orbitals with graphene electrodes. *Adv. Mater.* **30**, 1706322 (2018).
25. Y. Kim, T. J. Hellmuth, M. Burkle, F. Pauly, E. Scheer, Characteristics of amine-ended and thiol-ended Alkane single-molecule junctions revealed by inelastic electron tunneling spectroscopy. *ACS Nano* **5**, 4104–4111 (2011).
26. T. Zaba, A. Noworolska, C. M. Bowers, B. Breiten, G. M. Whitesides, P. Cyganik, Formation of highly ordered self-assembled monolayers of alkynes on Au(111) substrate. *J. Am. Chem. Soc.* **136**, 11918–11921 (2014).
27. T. M. Willey, A. L. Vance, T. van Buuren, C. Bostedt, L. J. Terminello, C. S. Fadley, Rapid degradation of alkanethiol-based self-assembled monolayers on gold in ambient laboratory conditions. *Surf. Sci.* **576**, 188–196 (2005).
28. M. H. Schoenfisch, J. E. Pemberton, Air stability of alkanethiol self-assembled monolayers on silver and gold surfaces. *J. Am. Chem. Soc.* **120**, 4502–4513 (1998).
29. N. Nerngchamnong, L. Yuan, D. C. Qi, J. Li, D. Thompson, C. A. Nijhuis, The role of van der Waals forces in the performance of molecular diodes. *Nat. Nanotechnol.* **8**, 113–118 (2013).
30. X. Chen, M. Roemer, L. Yuan, W. Du, D. Thompson, E. Del Barco, C. A. Nijhuis, Molecular diodes with rectification ratios exceeding 10^5 driven by electrostatic interactions. *Nat. Nanotechnol.* **12**, 797–803 (2017).
31. R. P. Sullivan, J. T. Morningstar, E. Castellanos-Trejo, R. W. Bradford, Y. J. Hofstetter, Y. Vaynzof, M. E. Welker, O. D. Jurchescu, Intermolecular charge transfer enhances the performance of molecular rectifiers. *Sci. Adv.* **8**, eabq7224 (2022).
32. S. Goswami, R. Pramanick, A. Patra, S. P. Rath, M. Foltin, A. Ariando, D. Thompson, T. Venkatesan, S. Goswami, R. S. Williams, Decision trees within a molecular memristor. *Nature* **597**, 51–56 (2021).
33. J. Li, S. J. Hou, Y. R. Yao, C. Y. Zhang, Q. Q. Wu, H. C. Wang, H. W. Zhang, X. Y. Liu, C. Tang, M. X. Wei, W. Xu, Y. P. Wang, J. T. Zheng, Z. C. Pan, L. X. Kang, J. Y. Liu, J. Shi, Y. Yang, C. J. Lambert, S. Y. Xie, W. J. Hong, Room-temperature logic-in-memory operations in single-metallofullerene devices. *Nat. Mater.* **21**, 917–923 (2022).
34. Y. L. Wang, Q. Zhang, H. P. A. G. Astier, C. Nickle, S. Soni, F. A. Alami, A. Borrini, Z. Y. Zhang, C. Honnigfort, B. Braunschweig, A. Leoncini, D. C. Qi, Y. M. Han, E. del Barco, D. Thompson, C. A. Nijhuis, Dynamic molecular switches with hysteretic negative differential conductance emulating synaptic behaviour. *Nat. Mater.* **21**, 1403–1411 (2022).
35. T. Schmaltz, A. Y. Amin, A. Khassanov, T. Meyer-Friedrichsen, H. G. Steinruck, A. Magerl, J. J. Segura, K. Voitchovsky, F. Stellacci, M. Halik, Low-voltage self-assembled monolayer field-effect transistors on flexible substrates. *Adv. Mater.* **25**, 4511–4514 (2013).
36. S. Park, G. Wang, B. Cho, Y. Kim, S. Song, Y. Ji, M. H. Yoon, T. Lee, Flexible molecular-scale electronic devices. *Nat. Nanotechnol.* **7**, 438–442 (2012).
37. Y. W. Jiang, Z. T. Zhang, Y. X. Wang, D. L. Li, C. T. Coen, E. Hwaun, G. Chen, H. C. Wu, D. L. Zhong, S. M. Niu, W. C. Wang, A. Saberi, J. C. Lai, Y. L. Wu, Y. Wang, A. A. Trotsyuk, K. Y. Loh, C. C. Shih, W. H. Xu, K. Liang, K. L. Zhang, Y. H. Bai, G. Gurusankar, W. P. Hu, W. Jia, Z. Cheng, R. H. Dauskardt, G. C. Gurtner, J. B. H. Tok, K. Deisseroth, I. Soltesz, Z. N. Bao, Topological supramolecular network enabled high-conductivity, stretchable organic bioelectronics. *Science* **375**, 1411–1417 (2022).
38. H. B. Akkerman, A. J. Kronemeijer, J. Harkema, P. A. van Hal, E. C. P. Smits, D. M. de Leeuw, P. W. M. Blom, Stability of large-area molecular junctions. *Org Electron* **11**, 146–149 (2010).
39. G. Puebla-Hellmann, K. Venkatesan, M. Mayor, E. Lortscher, Metallic nanoparticle contacts for high-yield, ambient-stable molecular-monolayer devices. *Nature* **559**, 232–235 (2018).
40. H. B. Akkerman, P. W. M. Blom, D. M. de Leeuw, B. de Boer, Towards molecular electronics with large-area molecular junctions. *Nature* **441**, 69–72 (2006).
41. C. M. Crudden, J. H. Horton, O. V. Ebralidze II, A. B. Zenkina, B. McLean, Z. Drevniok, H. B. She, N. J. Kraatz, T. Mosey, E. C. Seki, J. D. Keske, A. Leake, G. W. Rousina-Webb, Ultra stable self-assembled monolayers of N-heterocyclic carbenes on gold. *Nat. Chem.* **6**, 409–414 (2014).
42. D. T. Nguyen, M. Freitag, C. Gutheil, K. Sotthewes, B. J. Tyler, M. Bockmann, M. Das, F. Schluter, N. L. Doltsinis, H. F. Arlinghaus, B. J. Ravoo, F. Glorius, An arylazopyrazole-based N-heterocyclic carbene as a photoswitch on gold surfaces: Light-switchable wettability, work function, and conductance. *Angew. Chem. Int. Ed.* **59**, 13651–13656 (2020).
43. X. Qiu, V. Ivasyshyn, L. Qiu, M. Enache, J. Dong, S. Rousseva, G. Portale, M. Stohr, J. C. Hummelen, R. C. Chiechi, Thiol-free self-assembled oligoethylene glycols enable robust air-stable molecular electronics. *Nat. Mater.* **19**, 330–337 (2020).
44. T. Kondo, M. Yanagida, K. Shimazu, K. Uosaki, Determination of thickness of a self-assembled monolayer of dodecanethiol on Au(111) by angle-resolved X-ray photoelectron spectroscopy. *Langmuir* **14**, 5656–5658 (1998).
45. C. D. Bain, E. B. Troughton, T. T. Yu, J. Evall, G. M. Whitesides, R. G. Nuzzo, Formation of monolayer films by the spontaneous assembly of organic thiols from solution onto gold. *J. Am. Chem. Soc.* **111**, 321–335 (1989).
46. P.-Y. Blanchard, G. T. Kenfack, E. Levillain, C. Gautier, Self-assembled monolayers prepared from alkanethiols or dialkyl disulfides on Au: Evidence of influence of the anchoring group. *ChemistrySelect* **1**, 3171–3174 (2016).
47. J. M. Tour, L. Jones, D. L. Pearson, J. J. S. Lamba, T. P. Burgin, G. M. Whitesides, D. L. Allara, A. N. Parikh, S. V. Atre, Self-assembled monolayers and multilayers of conjugated thiols, .alpha.,.omega.-dithiols, and thioacetyl-containing adsorbates. Understanding attachments between potential molecular wires and gold surfaces. *J. Am. Chem. Soc.* **117**, 9529–9534 (1995).
48. M. I. Bethencourt, L. O. Srisombat, P. Chinwangso, T. R. Lee, SAMs on gold derived from the direct adsorption of alkanethioacetates are inferior to those derived from the direct adsorption of alkanethiols. *Langmuir* **25**, 1265–1271 (2009).
49. L. Jiang, L. Yuan, L. Cao, C. A. Nijhuis, Controlling leakage currents: The role of the binding group and purity of the precursors for self-assembled monolayers in the performance of molecular diodes. *J. Am. Chem. Soc.* **136**, 1982–1991 (2014).
50. A. Bashir, D. Kafer, J. Muller, C. Woll, A. Terfort, G. Witte, Selenium as a key element for highly ordered aromatic self-assembled monolayers. *Angew. Chem. Int. Ed.* **47**, 5250–5252 (2008).
51. A. Shaporenko, J. Mueller, T. Weidner, A. Terfort, M. Zharnikov, Balance of structure-building forces in selenium-based self-assembled monolayers. *J. Am. Chem. Soc.* **129**, 2232–2233 (2007).
52. F. K. Huang, R. C. Horton, D. C. Myles, R. L. Garrell, Selenolates as alternatives to thiolates for self-assembled monolayers: A SERS study. *Langmuir* **14**, 4802–4808 (1998).
53. A. Shaporenko, P. Cyganik, M. Buck, A. Terfort, M. Zharnikov, Self-assembled monolayers of aromatic selenolates on noble metal substrates. *J. Phys. Chem. B* **109**, 13630–13638 (2005).
54. A. Shaporenko, A. Ulman, A. Terfort, A. Zharnikov, Self-assembled monolayers of alkaneselenolates on (111) gold and silver. *J. Phys. Chem. B* **109**, 3898–3906 (2005).
55. C. K. Yee, A. Ulman, J. D. Ruiz, A. Parikh, H. White, M. Rafailovich, Alkyl selenide- and alkyl thiolate-functionalized gold nanoparticles: Chain packing and bond nature. *Langmuir* **19**, 9450–9458 (2003).
56. S. Mankefors, A. Grigoriev, G. Wendin, Molecular alligator clips: A theoretical study of adsorption of S, Se and S-H on Au(111). *Nanotechnology* **14**, 849–858 (2003).
57. J. Ossowski, G. Nascimbeni, T. Żaba, E. Verwüster, J. Rysz, A. Terfort, M. Zharnikov, E. Zojer, P. Cyganik, Relative thermal stability of thiolate- and selenolate-bonded aromatic monolayers on the Au(111) substrate. *J. Phys. Chem. C* **121**, 28031–28042 (2017).
58. J. Ossowski, T. Wachter, L. Silies, M. Kind, A. Noworolska, F. Blobner, D. Gnatek, J. Rysz, M. Bolte, P. Feulner, A. Terfort, P. Cyganik, M. Zharnikov, Thiolate versus selenolate: Structure, stability, and charge transfer properties. *ACS Nano* **9**, 4508–4526 (2015).
59. S. Y. Lee, E. Ito, H. Kang, M. Hara, H. Lee, J. Noh, Surface structure, adsorption, and thermal desorption behaviors of methaneselenolate monolayers on Au(111) from dimethyl diselenides. *J. Phys. Chem. C* **118**, 8322–8330 (2014).
60. K. Bandyopadhyay, K. Vijayamohanan, Formation of a self-assembled monolayer of diphenyl diselenide on polycrystalline gold. *Langmuir* **14**, 625–629 (1998).
61. A. Shaporenko, P. Cyganik, M. Buck, A. Ulman, A. Zharnikov, Self-assembled monolayers of semifluorinated alkaneselenolates on noble metal substrates. *Langmuir* **21**, 8204–8213 (2005).
62. S. Han, S. Seong, Y. J. Son, Y. Yokota, T. Hayashi, M. Hara, J. Noh, Formation and surface structures of highly ordered self-assembled monolayers of alkyl selenocyanates on Au(111) via ambient-pressure vapor deposition. *J. Phys. Chem. C* **124**, 26730–26740 (2020).
63. M. Wróbel, T. Żaba, E. Sauter, M. Krawiec, J. Sobczuk, A. Terfort, M. Zharnikov, P. Cyganik, Thermally stable and highly conductive SAMs on Ag substrate-the impact of the anchoring group. *Adv. Electron. Mater.* **7**, 2000947 (2021).
64. A. Krzykawska, M. Wrobel, K. Koziel, P. Cyganik, N-heterocyclic carbenes for the self-assembly of thin and highly insulating monolayers with high quality and stability. *ACS Nano* **14**, 6043–6057 (2020).
65. K. C. Liao, C. M. Bowers, H. J. Yoon, G. M. Whitesides, Fluorination, and tunneling across molecular junctions. *J. Am. Chem. Soc.* **137**, 3852–3858 (2015).
66. C. M. Bowers, D. Rappoport, M. Baghbanzadeh, F. C. Simeone, K.-C. Liao, S. N. Semenov, T. Żaba, P. Cyganik, A. Aspuru-Guzik, G. M. Whitesides, Tunneling across SAMs containing oligophenyl groups. *J. Phys. Chem. C* **120**, 11331–11337 (2016).
67. Z. J. Zuo, J. Li, P. D. Han, W. Huang, XPS and DFT studies on the autoxidation process of Cu sheet at room temperature. *J. Phys. Chem. C* **118**, 20332–20345 (2014).
68. Y. Kim, K. Yuan, B. R. Ellis, U. Becker, Redox reactions of selenium as catalyzed by magnetite: Lessons learned from using electrochemistry and spectroscopic methods. *Geochim. Cosmochim. Acta* **199**, 304–323 (2017).
69. R. Dronskowski, P. E. Blochl, Crystal orbital Hamilton populations (COHP) - Energy-resolved visualization of chemical bonding in solids based on density-functional calculations. *J. Phys. Chem.* **97**, 8617–8624 (1993).

70. V. L. Deringer, A. L. Tchougreeff, R. Dronskowski, Crystal orbital Hamilton population (COHP) analysis as projected from plane-wave basis sets. *J. Phys. Chem. A* **115**, 5461–5466 (2011).
71. S. Maintz, V. L. Deringer, A. L. Tchougreeff, R. Dronskowski, Analytic projection from plane-wave and PAW wavefunctions and application to chemical-bonding analysis in solids. *J. Comput. Chem.* **34**, 2557–2567 (2013).
72. J. L. Lin, Z. Cao, X. Y. Bai, N. Y. Chen, C. T. Li, X. W. Xiao, L. J. Wang, Y. Li, Molecular diodes with tunable threshold voltage based on π-extended tetrathiafulvalene. *Adv. Mater. Interfaces* **9**, 2201238 (2022).
73. N. Ma, Y. Li, H. P. Xu, Z. Q. Wang, X. Zhang, Dual redox responsive assemblies formed from diselenide block copolymers. *J. Am. Chem. Soc.* **132**, 442–443 (2010).
74. L. Wang, R. Liu, J. L. Gu, B. Song, H. Wang, X. Jiang, K. R. Zhang, X. Han, X. Q. Hao, S. Bai, M. Wang, X. H. Li, B. Q. Xu, X. P. Li, Self-assembly of supramolecular fractals from generation 1 to 5. *J. Am. Chem. Soc.* **140**, 14087–14096 (2018).
75. L. Yuan, L. Jiang, C. A. Nijhuis, The drive force of electrical breakdown of large-area molecular tunnel junctions. *Adv. Funct. Mater.* **28**, 1801710 (2018).
76. G. Kresse, J. Hafner, Ab initiomolecular dynamics for liquid metals. *Phys. Rev. B Condens. Matter* **47**, 558–561 (1993).
77. G. Kresse, J. Furthmuller, Efficiency of ab-initio total energy calculations for metals and semiconductors using a plane-wave basis set. *Comp. Mater. Sci.* **6**, 15–50 (1996).
78. G. Kresse, D. Joubert, From ultrasoft pseudopotentials to the projector augmented-wave method. *Phys. Rev. B* **59**, 1758–1775 (1999).
79. J. P. Perdew, K. Burke, M. Ernzerhof, Generalized gradient approximation made simple. *Phys. Rev. Lett.* **77**, 3865–3868 (1996).
80. H. J. Monkhorst, J. D. Pack, Special points for Brillouin-zone integrations. *Phys. Rev. B* **13**, 5188–5192 (1976).
81. S. Maintz, V. L. Deringer, A. L. Tchougreeff, R. Dronskowski, LOBSTER: A tool to extract chemical bonding from plane-wave based DFT. *J. Comput. Chem.* **37**, 1030–1035 (2016).
82. G. Henkelman, B. P. Uberuaga, H. Jonsson, A climbing image nudged elastic band method for finding saddle points and minimum energy paths. *J. Chem. Phys.* **113**, 9901–9904 (2000).
83. G. Henkelman, H. Jonsson, Improved tangent estimate in the nudged elastic band method for finding minimum energy paths and saddle points. *J. Chem. Phys.* **113**, 9978–9985 (2000).
84. H. Kondoh, I. Nakai, A. Nambu, T. Ohta, T. Nakamura, R. Kimura, M. Matsumoto, Dissociative and non-dissociative adsorption of selenophene on Au(111) depending on the preparation method. *Chem. Phys. Lett.* **350**, 466–472 (2001).
85. T. Sumi, H. Wano, K. Uosaki, Electrochemical oxidative adsorption and reductive desorption of a self-assembled monolayer of decanethiol on the Au(111) surface in KOH+ethanol solution. *J. Electroanal. Chem.* **550-551**, 321–325 (2003).
86. D. Hobara, K. Miyake, S.-I. Imabayashi, K. Niki, T. Kakiuchi, In-situ scanning tunneling microscopy imaging of the reductive desorption process of alkanethiols on Au(111). *Langmuir* **14**, 3590–3596 (1998).
87. D. F. Yang, C. P. Wilde, M. Morin, Studies of the electrochemical removal and efficient reformation of a monolayer of hexadecanethiol self-assembled at an Au(111) single crystal in aqueous solutions. *Langmuir* **13**, 243–249 (1997).
88. G. Che, Z. Li, H. Zhang, C. R. Cabrera, Voltammetry of defect sites at a self-assembled monolayer on a gold surface. *J. Electroanal. Chem.* **453**, 9–17 (1998).
89. C. Miller, P. Cuendet, M. Graetzel, Adsorbed .omega.-hydroxy thiol monolayers on gold electrodes: Evidence for electron tunneling to redox species in solution. *J. Phys. Chem.* **95**, 877–886 (1991).
90. M. D. Porter, T. B. Bright, D. L. Allara, C. E. D. Chidsey, Spontaneously organized molecular assemblies. 4. Structural characterization of n-alkyl thiol monolayers on gold by optical ellipsometry, infrared spectroscopy, and electrochemistry. *J. Am. Chem. Soc.* **109**, 3559–3568 (1987).
91. J. H. Xia, P. Zhao, K. Zheng, C. J. Lu, S. C. Yin, H. P. Xu, Surface modification based on diselenide dynamic chemistry: Towards liquid motion and surface bioconjugation. *Angew. Chem. Int. Ed.* **58**, 542–546 (2019).

Acknowledgments

Funding: N.C., Y.X., J.-L.L., and Y.L. thank the funding supports from the National Natural Science Foundation of China (22273045). P.Z. and H.X. thank the funding supports from the National Natural Science Foundation of China (52233012 and 21821001). R.L. and B.X. thank the funding supports from the NSF (ECCS 2010875). Y.L. and L.Z. also thank the funding supports from Tsinghua University Dushi Program and Initiative Scientific Research Program. We also acknowledge NCESBJ where the SAMs characterization was conducted. **Author contributions:** H.X. and Y.L. initiated the project and designed the experiments. N.C. prepared samples, performed surface characterization of samples, and conducted electrical measurements. S.L., N.C., and L.Z. did the theoretical calculations and co-wrote part of the calculations. P.Z. synthesized and characterized all the molecules. Y.X. prepared the Au-bottom electrodes. J.-L.L. performed part of the electrical measurement of S-SAMs. R.L. and B.X. prepared the mica-Au SAMs samples and performed STM imaging. N.C. and Y.L. analyzed experimental data and contributed mainly to the writing of the manuscript. C.A.N. provided suggestions to the manuscript. All authors discussed the results and data analysis and contributed to the writing of the manuscript. **Competing interests:** The authors declare that they have no competing interests. **Data and materials availability:** All data needed to evaluate the conclusions in the paper are present in the paper and/or the Supplementary Materials.

Submitted 26 February 2023
Accepted 14 September 2023
Published 18 October 2023
10.1126/sciadv.adh3412

ScienceAdvances

Extreme long-lifetime self-assembled monolayer for air-stable molecular junctions

Ningyue Chen, Shuwei Li, Peng Zhao, Ran Liu, Yu Xie, Jin-Liang Lin, Christian A. Nijhuis, Bingqian Xu, Liang Zhang, Huaping Xu, and Yuan Li

Sci. Adv. **9** (42), eadh3412. DOI: 10.1126/sciadv.adh3412